Journal of Computational Physics **179,** 400–425 (2002)
doi:10.1006/jcph.2002.7061

A Direct Simulation Method for Subsonic, Microscale Gas Flows

Quanhua Sun and Iain D. Boyd

Department of Aerospace Engineering, University of Michigan, Ann Arbor, Michigan 48109
E-mail: qsun@engin.umich.edu, iainboyd@engin.umich.edu

Received November 12, 2001; revised March 25, 2002

Microscale gas flows are the subject of increasingly active research due to the rapid advances in micro-electro-mechanical systems (MEMS). The rarefied phenomena in MEMS gas flows make molecular-based simulations desirable. However, it is necessary to reduce the statistical scatter in particle methods for microscale gas flows. In this paper, the development of an information preservation (IP) method is described. The IP method reduces the statistical scatter by preserving macroscopic information of the flow in the particles and the computational cells simulated in the direct simulation Monte Carlo (DSMC) method. The preserved macroscopic information of particles is updated during collisions and is then modified to include the pressure field effects excluded in the collisions. An additional energy transfer model is proposed to describe the energy flux across an interface, and a collision model is used to redistribute the information after both particle–particle and particle–surface collisions. To validate the IP method, four different flows are simulated and the solutions are compared against DSMC results. The results from the IP method generally agree very well with the DSMC results for steady flows and low frequency unsteady flows ranging from the near-continuum regime to the free-molecular regime.

Key Words: information preservation method; direct simulation Monte Carlo method; microscale gas flows; subsonic flows; rarefied gas dynamics.

I. INTRODUCTION

Simulation of gas flow around microscale structures is gaining importance due to the rapid development of micro-electro-mechanical systems (MEMS) [1, 2]. Previous investigations [3–5] have shown that the fluid behavior around MEMS is different from the macroscopic counterparts. However, experimental study of microscale gas flows is made inherently difficult by the small physical dimensions and has been mainly limited to simple structures, such as micro channels and micro nozzles [3, 6]. Numerical modeling is also a challenge

0021-9991/02 $35.00

because the MEMS components operate in a variety of flow regimes covering the continuum, slip, and transition regimes.

The flow regimes can be characterized by the Knudsen number (Kn, the ratio of gas mean free path λ to a characteristic microfluidic length L). Typically, the continuum regime is in the range of $\mathrm{Kn} \leq 0.01$, the slip regime is $0.01 \leq \mathrm{Kn} \leq 0.1$, and the Knudsen number of the transition regime is between 0.1 and 10. For air flows in the slip regime, the air in contact with the body surface may have a nonzero tangential velocity relative to the surface, and traditional computational fluid dynamic techniques can be used only if a slip wall condition is adopted instead of the usual nonslip boundary condition. However, for transition flows ($\lambda \sim L$), collisions between molecules and collisions of molecules with the wall have the same order of probability. In this case, general kinetic models are required to include the rarefied phenomena.

The direct simulation Monte Carlo (DSMC) method is one of the most successful particle simulation methods for rarefied gas flows [7, 8]. Several review articles about the DSMC method are available [9–11]. However, the DSMC method cannot effectively reduce the statistical scatter encountered in microscale flows, which gives a very large noise-to-information ratio since the flows usually have low speed and/or small temperature variation. For microscale flows, several particle methods have been proposed [12–15]. Fan and other researchers have developed an information preservation (IP) method for low speed rarefied gas flows [12, 13, 16–18]. The IP method uses the molecular velocities of the DSMC method as well as physical information that describes the collective behavior of the large number of molecules that a simulated particle represents, and additional treatment is used to update the physical information. Meanwhile, Pan and co-workers proposed a molecular block model DSMC method based on the relationship between the statistical scatter and the molecular mass [15]. In their method, the reference diameter and number density of the so-called big molecule are determined by ensuring that the mean free path and dynamic viscosity of the big molecule are equal to those of the real constituent molecules. However, both methods have not been tested for general microscale flows.

In the present paper, the information preservation method for general 2D microscale flows is developed. The preserved macroscopic information is first solved in a similar way to the microscopic information in the DSMC method and is then modified to include the pressure effects. With two proposed models, the IP method is applied to simulate four different flows. The main purpose of this paper is to demonstrate the validity of the proposed implementation of the IP method since previous papers have shown its ability in decreasing the statistical scatter for particle methods.

II. INFORMATION PRESERVATION METHOD

2.1. Background and Basic Idea

The information preservation method, first proposed by Fan and Shen [12], was used to overcome the problem of statistical scatter in the DSMC method for low-speed, constant density flow systems. It achieved great success for several unidirectional transitional gas flows as shown in [13], including Couette flow, Poiseuille flow, and the Rayleigh problem. This method was later developed by Cai *et al.* in simulating low-speed microchannel flows [16] and investigating the flows around a NACA0012 airfoil [18] by calculating the macroscopic velocity and solving the density flow field from the continuity equation. However,

the isothermal assumption used in their implementation limits the further applications of the method. In this paper, the IP method is developed for general microscale gas flows, and models are proposed when necessary.

The basic idea of the IP method is based on the following consideration. It is generally required that each particle simulated in the DSMC method represents an enormous number (10^8–10^{25}) of real molecules, and the velocity of these particles can be split into two parts

$$U = V + C, \tag{1}$$

where U is the particle velocity, V is the mean molecular velocity, and C is the thermal velocity. In other words, the particle carries the sum of the macroscopic velocity of a gas flow $V(V = \bar{U})$ and the velocity scatter C ($\bar{C} = 0$). The information preservation method aims to preserve and update the macroscopic information of a gas flow, intending to reduce the statistical scatter inherent in particle methods.

In general, the particle carries the sum of the gas macroscopic information and the information scatter. From this view, we intend to additionally preserve the energy information (represented by temperature T) in simulated DSMC particles for general gas flows.

2.2. Principle

The general equation for dilute gas flows is the Boltzmann equation

$$\frac{\partial}{\partial t}(nf) + \vec{c} \cdot \frac{\partial}{\partial \vec{r}}(nf) + \vec{F} \cdot \frac{\partial}{\partial \vec{c}}(nf) = \int_{-\infty}^{\infty} \int_{0}^{4\pi} n^2 (f^* f_1^* - f f_1) c_r \sigma \, \mathrm{d}\Omega \, \mathrm{d}\vec{c}_1, \tag{2}$$

where f is the velocity distribution function, n is the number density, t is the time, $\vec{r}$ is the physical space vector, $\vec{c}$ is the velocity space vector, $\vec{F}$ is the external force per unit mass, c_r is the relative speed between a molecule of class $\vec{c}$ and one of class $\vec{c}_1$, and $\sigma \mathrm{d}\Omega$ is the differential cross section for the collision of a molecule of class $\vec{c}$ with one of class $\vec{c}_1$ such that their postcollision velocities are $\vec{c}^*$ and $\vec{c}_1^*$, respectively. Due to the complexity of this equation, especially the collision term on the right-hand side of the equation, the direct simulation Monte Carlo method is often used to simulate dilute gas flows. The DSMC method does not solve the Boltzmann equation, however, it does provide solutions that are consistent with the Boltzmann equation. It is assumed that the molecule motion can be decoupled from the molecule collisions and the gas can be represented by a set of tracking particles (representative molecules) for dilute gas flows. The DSMC method tracks the particles with their individual location, velocity, and internal energy, and models both particle–particle and particle–surface collisions probabilistically. An important assumption for the IP method is that the particles simulated in the DSMC method can carry the macroscopic information of the flow field and the macroscopic information is changed during collisions. Then the key part of the IP method is how to evaluate particle collisions for the macroscopic information.

For low-speed, constant density flow systems, Fan and Shen [12] used the following simple collision model for the preserved macroscopic velocity

$$V_1'' = V_2'' = (V_1' + V_2')/2, \tag{3}$$

where superscripts $'$ and $''$ denote pre- and postcollision, and subscripts 1 and 2 denote particles 1 and 2 in the collision pair. However, for general flows, it is quite a challenge to model the effect of particle collisions on all macroscopic information. It is believed that particle collisions lead to momentum and energy exchange. Hence, it is necessary to preserve the macroscopic velocity and temperature in particles. Further, if we consider continuum flows, it is clear that the macroscopic velocity and temperature are changed not only by the momentum and energy exchange but also by the pressure field. Therefore, for the IP method, two steps are required. One is the collision and movement step where the whole DSMC algorithm is applied to both the original DSMC variables and the preserved macroscopic information, and the other is the modification step, which is used to include the pressure effects. During the modification step, the following equations are solved with the help of the macroscopic information that is preserved in the computational cells,

$$\frac{\partial V_i}{\partial t} = -\frac{1}{\rho_c}\frac{\partial p_c}{\partial r_i} \tag{4}$$

$$\frac{\partial}{\partial t}\left(\frac{V_i \cdot V_i}{2} + \frac{\xi \cdot R \cdot T}{2}\right) = -\frac{1}{\rho_c}\frac{\partial}{\partial r_i}(V_{i,c} \cdot p_c), \tag{5}$$

where p is the pressure, ρ is the mass density, R is the specific gas constant, ξ is the number of internal degrees of freedom of molecules, and the subscript c denotes the macroscopic information for the computational cells. Variables ρ_c and p_c are calculated using Eqs. (6) and (7), respectively, and T_c and $V_{i,c}$ are sampled from the particles within the cell, which will be detailed in the implementation section.

$$\frac{\partial \rho_c}{\partial t} = -\frac{\partial}{\partial r_i}(\rho_c \cdot V_{i,c}) \tag{6}$$

$$p_c = \rho_c \cdot R \cdot T_c. \tag{7}$$

2.3. Additional Energy Transfer Model

As can be seen, the IP method is based on the microscopic movement of the particles simulated in the DSMC method. There is a contradiction between the real flux and the IP representation about the energy flux across an interface (e.g., a surface of a computational cell). The net energy flux across an interface is zero in stationary equilibrium flows. However, the average translational energy carried by a molecule across an interface is $2kT$, which is different from $3kT/2$, the average translational energy of a molecule. Here k is the Boltzmann constant. In equilibrium flows, this difference arises because the translational energy flux of the component normal to the interface is twice the flux of the component in the other directions. For general nonequilibrium flows, the difference here cannot be balanced. Hence, it is necessary to introduce additional energy flux for the IP method. In the literature, several attempts have been made for general flows [20, 21], but the results are far from satisfactory. In this paper, an approximate model is proposed as follows.

The current model aims to capture the net energy flux across an interface instead of recovering the microscopic energy for every particle. A simple example may illustrate this model. A plate separates a gas with one part at temperature T_1 and the other at T_2. After the plate is removed, some molecules described by T_1 will move to the other side. On average, the T_1 particles will transfer $3kT_1/2$ plus an additional $kT_1/2$ to the other side, and vice versa.

Assuming that the number of particles crossing in each direction is equal, then the net energy flux based on the moving particles is $3k(T_1 - T_2)/2$ plus the additional $k(T_1 - T_2)/2$. This process is modeled by assuming that the T_1 particles will transfer $3kT_1/2$ plus an additional $k(T_1 - T_{ref})/2$ to the other side, and the T_2 particles will transfer $3kT_2/2$ plus an additional $k(T_2 - T_{ref})/2$ to the other side, where T_{ref} is a reference temperature. Therefore, the IP method captures the net energy flux across an interface in an average sense.

In the IP method, when a particle crosses an interface, it carries an additional energy that is to be determined in some way, and the particle "borrows" some energy from other particles to satisfy the conservation of energy. As illustrated in the example, the additional energy is taken as $k(T - T_{ref})/2$, where T_{ref} is very close to the preserved temperature T of the particle. It is clear that part of the additional energy $kT_{ref}/2$ of one particle must be balanced by another particle such that the net flux across an interface can be correctly modeled. For stationary gas flows, the number of particles crossing in each direction is the same. Hence, the reference temperature can be taken as the temperature on the interface that a particle will cross, which can be interpolated from the preserved temperatures of two neighboring cells. Then the effect of the additional energy $kT_{ref}/2$ of one particle will be balanced by another particle that will cross the same interface from the other direction. For steady flows with small bulk velocity, however, the number of particles crossing in each direction is not the same, but very close. The additional energy $kT_{ref}/2$ of most of the particles crossing one interface can be balanced by other particles crossing the same interface from the other side, and the additional energy $kT_{ref}/2$ of the particles that are not balanced needs to be balanced by another means. Statistically, there is another molecule leaving a computational cell from one interface when a molecule enters the cell through another interface for steady flows. Therefore, the additional energy $kT_{ref}/2$ of the particles that enter a cell from one interface and are not balanced by the above means can be approximately balanced by particles leaving the cell from other interfaces because the difference of the reference temperatures (the flow temperatures on different interfaces) is relatively small. Hence, the additional energy transfer model can model the net energy flux approximately for steady flows. For unsteady flows, the model can also be a good approximation if the frequency is low or the temperature variation is small. In the implementation, the IP method preserves an additional variable T_a for particles to describe the additional energy $k(T - T_{ref})/2$ as $\xi kT_a/2$. As stated earlier, the additional energy is borrowed from other particles, so a new variable $T_{a,c}$ is preserved for cells to record the borrowed energy as $\xi kT_{a,c}/2$. At the end of each time step, the borrowed energy is evenly provided by all the particles in the cell to maintain the conservation of energy.

2.4. General Implementation

For subsonic, microscale flows, nonequilibrium between the translational energy and internal energy is not significant. Hence, only one temperature is used to denote the internal energy. In our 2D parallel IP code that is based on a parallel optimized DSMC code named "MONACO" [19], velocity components V_x, V_y and temperatures T, T_a are preserved for each simulated particle. Velocity components $V_{x,c}$, $V_{y,c}$, temperatures T_c, $T_{a,c}$, and density ρ_c are preserved for each computational cell.

The general implementation of the IP procedures (based on the DSMC procedures) can be summarized as follows (see also Fig. 1):

(1) Initialization: The information for all the particles and cells is initialized by the ambient conditions after the computational domain is set up, while T_a and $T_{a,c}$ are set to zero.

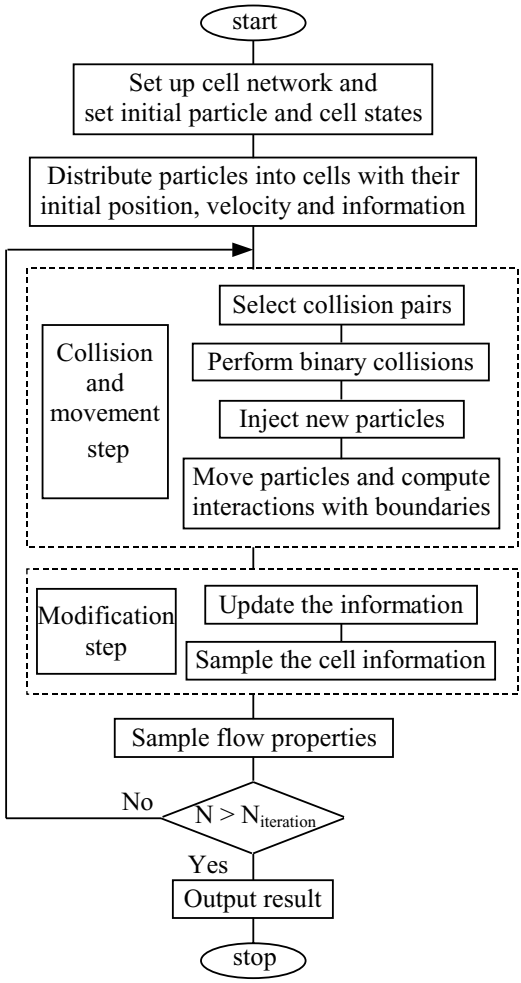

FIG. 1. DSMC-IP flowchart.

In each time step, one collision and movement step and one modification step are executed to update the preserved information. The collision and movement step is decoupled as a particle collision step and a particle movement step according to the usual DSMC procedures.

(2) Particle collision step: Particles are selected at random to make pairs, and binary collisions are performed for a subset of these pairs based on the usual DSMC procedures. It is believed that collisions lead particles to be in an equilibrium state; hence the preserved information of particles tends to be the same after collisions. Hence a simple collision model is given as

$$V''_{i,1} = V''_{i,2} = (V'_{i,1} + V'_{i,2})/2 \tag{8}$$

$$T''_1 = T''_2 = (T'_1 + T'_2)/2 + \lfloor (V'_{x,1} - V'_{x,2})^2 + (V'_{y,1} - V'_{y,2})^2 \rfloor / (4 \cdot \xi \cdot R) \tag{9}$$

$$T''_{a,1} = T''_{a,2} = (T'_{a,1} + T'_{a,2})/2. \tag{10}$$

However, the above model is too simple to simulate the viscosity and thermal conductivity correctly. A modified model will be proposed later.

(3) Particle movement step: Particles are moved with the molecular velocity as in the DSMC method. The preserved information of particles may change when particles interact with interfaces. Possible particle–interface interactions are:

(3a) Particles migrate from one cell to another. When particle j moves from cell k to another cell, momentum and energy transfer occurs, and additional energy transfer is required as stated in Section 2.3. The preserved additional energy for the particle and for the cell are adjusted as

$$T'_{a,j} = (T_j - T_{ref})/\xi \tag{11}$$

$$T'_{a,c,k} = T_{a,c,k} + T_{a,j} - T'_{a,j}, \tag{12}$$

where, T_{ref} is the interface temperature interpolated from the preserved cell temperatures of neighboring cells.

(3b) Particles leave or enter the computational domain. If a particle leaves the computational domain, the preserved information of the particle is lost along with the particle itself. As in the DSMC method, new particles may enter into the computational domain, and these particles are assigned information according to the boundary condition with $T_a = 0$.

(3c) Particles reflect from a symmetric boundary. When a particle reaches a symmetric boundary, it reflects from the boundary. The normal velocity component is reversed, and the parallel velocity component remains unchanged.

(3d) Particles reflect from a wall. The preserved information of particles collided with a wall is set in accordance with the collective behavior of a large number of real molecules. Namely, if it is a specular reflection, only the normal velocity component will be reversed. However, if it is a diffuse reflection, the preserved velocity and temperature of the reflected particles are set to the wall velocity and temperature. Also, the preserved additional temperature is changed.

For specular reflection:

$$T'_{a,j} = -T_{a,j} \tag{13}$$

$$T'_{a,c,k} = T_{a,c,k} + T_{a,j} - T'_{a,j}. \tag{14}$$

For diffuse reflection:

$$T''_{a,j} = (T_j - T_{ref})/\xi \tag{15}$$

$$T'_{a,c,k} = T_{a,c,k} + T_{a,j} - T''_{a,j} \tag{16}$$

$$T'_{a,j} = (T_w - T_{ref})/\xi. \tag{17}$$

Here, $T''_{a,j}$ denotes the additional temperature of the particle when it is "absorbed" by the wall. And $T_{ref} = \sqrt{T_j \cdot T_w}$, the constant gas temperature of collisionless flow between two plates with one at T_j and the other at T_w [23].

After the collisions and movements of particles are considered, the additional energy preserved by the cell k is shared across all N_p particles in the cell:

$$T'_j = T_j + T_{a,c,k}/N_p \tag{18}$$

$$T'_{a,c,k} = 0. \tag{19}$$

(4) Modification step: The preserved information of particles is modified by the pressure field during the modification step. Equations (4) and (5) are solved using a finite volume method:

$$\frac{\partial V_i}{\partial t} = -\frac{1}{\rho_c}\frac{1}{A}\oint_{cell} p_c \cdot n_i \, dl \tag{20}$$

$$\frac{\partial}{\partial t}\left(\frac{V_i \cdot V_i}{2} + \frac{\xi \cdot R \cdot T}{2}\right) = -\frac{1}{\rho_c}\frac{1}{A}\oint_{cell} (p_c \cdot V_{i,c} n_i) \, dl \tag{21}$$

$$V_i^{t+\Delta t} - V_i^t = -\frac{\Delta t}{\rho_c}\frac{1}{A}\oint_{cell} p_c \cdot n_i \, dl \tag{22}$$

$$\left(\frac{V_i \cdot V_i}{2} + \frac{\xi \cdot R \cdot T}{2}\right)^{t+\Delta t} - \left(\frac{V_i \cdot V_i}{2} + \frac{\xi \cdot R \cdot T}{2}\right)^{t} = -\frac{\Delta t}{\rho_c}\frac{1}{A}\oint_{cell} (p_c \cdot V_{i,c} n_i) \, dl. \tag{23}$$

In the above equations, A is the area of the cell, dl is the edge element of the cell, and $\vec{n}$ is the unit vector normal to the cell edge. The integrals are integrated over all cell edges. The cell information on cell edges is linearly interpolated using the information of the neighboring cells. To avoid statistical effects due to the number fluctuation of particles in a cell in Eqs. (20) and (21), the density ρ_c is replaced by the ratio of the real mass of the total represented molecules in the cell to the volume of the cell. For example,

$$\frac{\partial V_{i,j}}{\partial t} = -\frac{1}{\rho_c}\frac{1}{A}\oint_{cell} p_c \cdot n_i \, dl = -\frac{1}{N_p W_p m/\mathrm{Vol}}\frac{1}{A}\oint_{cell} p_c \cdot n_i \, dl \tag{24}$$

or

$$\sum_j^{N_p} \frac{1}{\mathrm{Vol}}\frac{\partial (W_p m V_{i,j})}{\partial t} = -\frac{1}{A}\oint_{cell} p_c \cdot n_i \, dl, \tag{25}$$

where subscript j denotes particle j in the cell, and W_p is the number of gas molecules represented by one particle. It is clear that the number fluctuation of particles in a cell does not affect the total pressure effects for all the particles in the cell.

(5) Update cell information: After the preserved information of particles is updated, the preserved information for cells is updated by averaging the information of all N_p particles in the cell.

$$V'_{i,c} = \sum_{j=1}^{N_p}\left(\frac{V_{i,j}}{N_p}\right) \tag{26}$$

$$T'_c = \sum_{j=1}^{N_p}\left(\frac{T_j + T_{a,j}}{N_p}\right). \tag{27}$$

The density is updated by Eq. (6). Again, it is solved by a finite volume method:

$$\frac{\partial \rho_c}{\partial t} = -\frac{1}{A}\oint_{cell} (\rho_c \cdot V_{i,c} \cdot n_i) \, dl. \tag{28}$$

(6) Sample flow properties: The flow properties are obtained by using time or ensemble averaging of the preserved information. The flow velocity $V_{i,f}$, flow temperature T_f, and flow density ρ_f are calculated as

$$V_{i,f} = \sum_{t=1}^{N_{step}} \left(\frac{V_{i,c,t}}{N_{step}} \right) \tag{29}$$

$$T_f = \sum_{t=1}^{N_{step}} \left(\frac{T_{c,t}}{N_{step}} + \frac{1}{N_{step} \cdot \xi \cdot R} \left(\sum_{j=1}^{N_{p,t}} \frac{V_{i,t,j} \cdot V_{i,t,j}}{N_{p,t}} - \left(\sum_{j=1}^{N_{p,t}} \frac{V_{i,t,j}}{N_{p,t}} \right)^2 \right) \right) \tag{30}$$

$$\rho_f = \sum_{t=1}^{N_{step}} \left(\frac{\rho_{c,t}}{N_{step}} \right). \tag{31}$$

In the above equations, i is the only index using the Einstein summation convention. The following are the expressions for the pressure p_w and shear stress τ_w on the wall, and heat flux q_w to the wall

$$p_w = p_c + \frac{\sum_{j=1}^{N_s} m\left(V_{n,j}^{re} - V_{n,j}^{in}\right)}{t_s \cdot \Delta A} \tag{32}$$

$$\tau_w = \frac{\sum_{j=1}^{N_s} m\left(V_{\tau,j}^{in} - V_{\tau,j}^{re}\right)}{t_s \cdot \Delta A} \tag{33}$$

$$q_w = \frac{\sum_{j=1}^{N_s} \left(\frac{1}{2} m V_{i,j}^2 + \frac{\xi}{2} k\left(T_j + T_{a,j}\right)\right)^{in} - \sum_{j=1}^{N_s} \left(\frac{1}{2} m V_{i,j}^2 + \frac{\xi}{2} k\left(T_j + T_{a,j}\right)\right)^{re}}{t_s \cdot \Delta A}, \tag{34}$$

where N_s is the total number of molecules hitting the wall element during t_s, ΔA is the area of the wall element, p_c is the pressure in the neighboring cell, subscript n denotes the normal velocity component, subscript τ denotes the tangential velocity component, and superscripts *in* and *re* denote the values before and after the wall element is struck, respectively.

For steady flows, steps (2)–(5) are repeated until the flow reaches a steady state. Then steps (2)–(5) are further repeated for the desired sampling size, and step (6) is used to obtain the final results. For unsteady flows, repeat steps (1)–(6) for the desired sampling size using ensemble averaging.

2.5. Viscosity and Thermal Conductivity

Numerical tests show that the simple collision model described in Section 2.4 (Step 2) cannot correctly simulate the viscosity and thermal conductivity of the flows. In Fan and Shen's paper [13], molecular diameters for the IP method are adjusted according to experimental data. Thus the molecular diameters for the IP method and for the DSMC method are different. Then the DSMC collisions with the molecular diameter for the IP method may not be correct, which will affect the results from the IP method.

Hence, the simple collision model needs to be modified. The preserved macroscopic information for two collision particles will not be the same after one particle collision. It will depend on the relative speed of the two particles, the deflection angle in the collision plane, and so on. A detailed mechanism for the IP method is then very difficult to obtain. Thus, a phenomenological model for the distribution of the information for the two particles is proposed based on the deflection angle in the collision plane,

$$V''_{i,1} = \frac{1 + C_\mu \cdot \cos(\theta)}{2} V'_{i,1} + \frac{1 - C_\mu \cdot \cos(\theta)}{2} V'_{i,2} \tag{35}$$

$$V''_{i,2} = \frac{1 - C_\mu \cdot \cos(\theta)}{2} V'_{i,1} + \frac{1 + C_\mu \cdot \cos(\theta)}{2} V'_{i,2} \tag{36}$$

$$\begin{aligned} T''_1 = {} & \frac{1 + C_\kappa \cdot \cos(\theta)}{2} T'_1 + \frac{1 - C_\kappa \cdot \cos(\theta)}{2} T'_2 \\ & + [(V'_{x,1} - V'_{x,2})^2 + (V'_{y,1} - V'_{y,2})^2]/(4 \cdot \xi \cdot R) \end{aligned} \tag{37}$$

$$\begin{aligned} T''_2 = {} & \frac{1 - C_\kappa \cdot \cos(\theta)}{2} T'_1 + \frac{1 + C_\kappa \cdot \cos(\theta)}{2} T'_2 \\ & + \left(1 - C_\mu^2 \cdot \cos^2\theta\right) \cdot [(V'_{x,1} - V'_{x,2})^2 + (V'_{y,1} - V'_{y,2})^2]/(4 \cdot \xi \cdot R) \end{aligned} \tag{38}$$

$$T''_{a,1} = \frac{1 + C_k \cdot \cos(\theta)}{2} T'_{a,1} + \frac{1 - C_k \cdot \cos(\theta)}{2} T'_{a,2} \tag{39}$$

$$T''_{a,2} = \frac{1 - C_k \cdot \cos(\theta)}{2} T'_{a,1} + \frac{1 + C_k \cdot \cos(\theta)}{2} T'_{a,2}, \tag{40}$$

where C_μ and C_κ are assumed to be constants depending on gas species, and θ is the deflection angle after collision in the collision plane. Table I lists the values of C_μ and C_κ determined by numerical experiments for five gases (He, Ar, N_2, O_2, and air) with the variable hard sphere (VHS) model [8]. Low speed Couette flows are used to determine the value of C_μ. Two plates at 273 K are separated by 1 m, with one at rest and the other with a parallel velocity of 1 m/s. C_μ is determined when the numerical shear stress agrees with the theoretical result ($\tau = \mu \partial u/\partial y$, experimental data [22] is used for the viscosity coefficient μ) when the Knudsen number of the flow is 0.01. Table II lists the shear stress distributions for the five gases in these Couette flows. The relation between the viscous coefficient and the gas temperature is shown in Fig. 2. The agreement between the numerical result and theory [8] ($\mu \propto T^\omega$) is satisfactory. These data indicate that C_μ is a constant. Table III lists the heat flux distributions in similar Couette flows. In this case, both plates are at rest, with one at 173 K and the other at 373 K. It is difficult to obtain an exact theoretical result since the temperature distribution is nonlinear and the flow exhibits some nonequilibrium phenomena. Hence, the averaged heat flux from the DSMC method is used to determine C_κ for the IP method.

TABLE I
Values of C_μ and C_κ for VHS Molecular Model

	He	Ar	N_2	O_2	Air
C_μ	−0.15	−0.18	−0.25	−0.21	−0.21
C_κ	1.15	1.28	0.87	0.87	0.87

TABLE II
Shear Stress Distributions ($\times 10^5$ N/m^2) for Five Gases in Couette Flows
(Kn = 0.01, U_w = 1 m/s, T = 273 K)

y/L	He	Ar	N_2	O_2	Air
0.1	1.834	2.067	1.616	1.879	1.683
0.2	1.834	2.067	1.617	1.878	1.682
0.3	1.834	2.069	1.617	1.878	1.681
0.4	1.834	2.071	1.618	1.878	1.681
0.5	1.834	2.072	1.621	1.877	1.681
0.6	1.833	2.073	1.620	1.880	1.682
0.7	1.833	2.075	1.618	1.879	1.681
0.8	1.832	2.074	1.615	1.876	1.678
0.9	1.833	2.069	1.616	1.875	1.681
Theory	1.824	2.066	1.616	1.873	1.678

2.6. Advantages and Disadvantages of the IP Method

The IP method preserves the information of the flow, which contains much less statistical scatter compared with the DSMC method for low speed flows. In DSMC, the statistical scatter comes directly from the thermal movement of particles. In IP, the thermal movement of particles causes scatter only at the macroscopic information level. In [13], the IP method reduced the sampling size required by a regular DSMC method for low speed flows by four orders of magnitude. This is a tremendous gain in computational time, which can lead to effective use of the IP method for microfluidic and MEMS simulations. Another

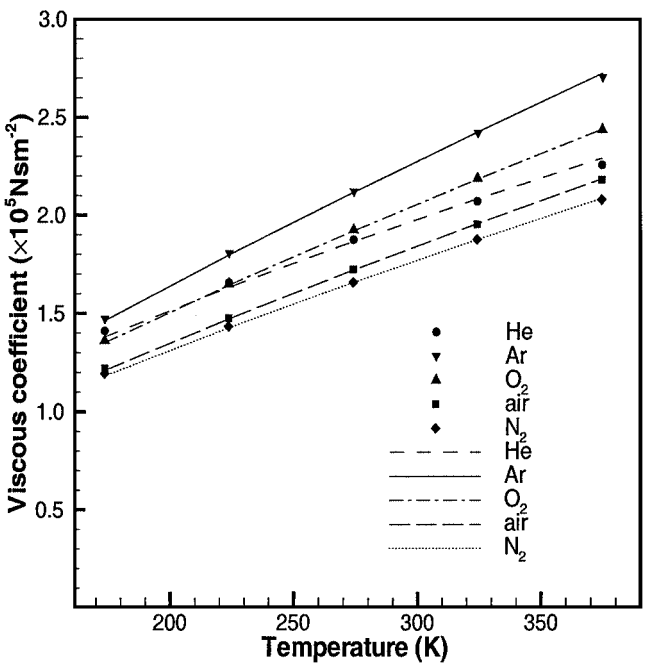

FIG. 2. Relation of viscous coefficient of five gases versus temperature (symbol: IP, line: theory $\mu \propto T^{\omega}$).

TABLE III
Heat Flux Distributions (W/m^2) for Five Gases in Couette Flows
(Kn = 0.01, $T_{w,1}$ = 173 K, $T_{w,2}$ = 373 K)

y/L	He	Ar	N_2	O_2	Air
0.1	26.18	3.080	4.333	4.366	4.305
0.2	26.21	3.080	4.330	4.363	4.302
0.3	26.22	3.080	4.334	4.362	4.307
0.4	26.23	3.083	4.332	4.361	4.300
0.5	26.24	3.077	4.333	4.377	4.301
0.6	26.26	3.080	4.342	4.370	4.301
0.7	26.27	3.083	4.337	4.366	4.302
0.8	26.29	3.083	4.337	4.362	4.299
0.9	26.29	3.084	4.337	4.360	4.314
DSMC	26.27	3.083	4.322	4.357	4.310

advantage of the IP method is that the macroscopic values of the flow field are known at any time, since the cell information is sampled for each time step. This helps the application of effective boundary conditions for the DSMC method for low speed flows, which improves the application of the DSMC method.

The IP method preserves more information than the DSMC method. Hence the implementation of the IP method is more complicated, and it requires more memory [16]. Generally, there is no stability criterion for the DSMC method. However, because of the modification step (Eqs. (4)–(6)) in the IP method, the time step cannot be large and the particle number in a cell cannot be small to control the statistical scatter for the equations to be solved correctly.

III. EXAMPLES OF FLOW SIMULATIONS

In previous studies, the IP method has exhibited the ability to reduce the statistical scatter in the DSMC method. In the present paper, the validity of the IP method is investigated. For microscale gas flows, there are few experimental data and simulation results in the literature. Hence, the DSMC method is used to compare with the IP results. However, the flow velocity and/or temperature variation of flows cannot be small to obtain the DSMC results with reasonable statistical scatter. Four different flow problems are chosen to assess the IP scheme. In the first example, flows between two plates at different temperatures, the IP method exhibits its ability to simulate problems with large temperature variation. Secondly, the IP method simulates a high speed Couette flow. The balance between the energy dissipation and thermal conductivity is investigated at different Knudsen numbers. Then a general Rayleigh problem is studied, which reveals a limitation of the IP method. The final example, flow over a NACA0012 airfoil, illustrates the application of the IP method to general two-dimensional problems.

To obtain results with small statistical scatter, both the DSMC and the IP methods require a certain number of sampling particles. For the DSMC method, the results are sampled from the microscopic velocity of the simulated particles. Hence it requires a large sampling size for low speed flows to get meaningful results. The sampling size is not sensitive to the Knudsen number of the flow as collisions still keep the microscopic velocity of the particles at the same level. For the IP method, it is possible to obtain smooth results with a small

sampling size because each particle carries the macroscopic information. However, it is very sensitive to the Knudsen number of the flow because particle collisions smooth the preserved macroscopic information of the particles. Therefore, the IP method needs very few time steps to obtain meaningful results for low speed gas flows with small Knudsen number. In the first three examples, the computational domain is divided into 200 cells. To get meaningful results, the DSMC method needs about 100,000 particles per cell. For the same level of results, the IP method only needs about 1000 particles per cell for flows with Kn = 0.01 and 10,000 particles per cell for flows with Kn = 100. For the results given below, a much larger sample size (20,000,000 particles per cell for examples 1 and 2, and 5,000,000 particles per cell for example 3) is used for both methods because it is better to use good smooth results to validate the method and because a single code is used where both results are obtained at the same time.

3.1. Flows between Two Plates at Different Temperatures

The simulation of energy transport is a difficult part in the IP method. Rarefied gas flow between two plates at different temperatures is one of the most fundamental problems in rarefied gas dynamics, which can test the energy transport in the IP method. In Fig. 3, two plates at rest are separated by 1 m, with one at 173 K and the other at 373 K. The density of the argon gas is selected such that the Knudsen number of the flows at 273 K ranges from 0.01 to 100.

Figure 4 shows the temperature profiles at different Knudsen numbers for the IP method and the DSMC method when the thermal accommodation coefficient is 1.0. At the Knudsen numbers of 0.01, 0.1, 1.0, and 100, excellent agreement is obtained between the IP and the DSMC results. The difference between the results from two methods when the Knudsen number is 10, however, is relatively small for such a strongly nonequilibrium flow. Figure 5 shows the heat flux for the IP method and the DSMC method. Again, excellent agreement is obtained. The IP method is also examined for different wall conditions when the Knudsen number is 0.01 and 1.0. When the Knudsen number is 0.01, the thermal accommodation coefficient for both plates is set as 1.0, 0.8, 0.6, 0.4, and 0.2, respectively. For the Kn = 1.0 case, several combinations of the thermal accommodation coefficient of the plates are used to further check the effects of the wall condition. As can be seen from Figs. 6 and 7, the agreement between the IP results and the DSMC results is also very good.

3.2. High Speed Couette Flow

It is critical that the viscosity and thermal conductivity can be simulated correctly by the IP method. A good example for this kind of verification is a high speed Couette flow.

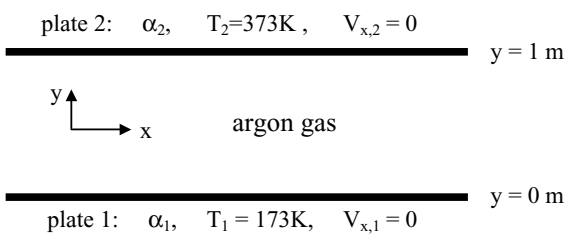

FIG. 3. Schematic diagram for the thermal Couette flow.

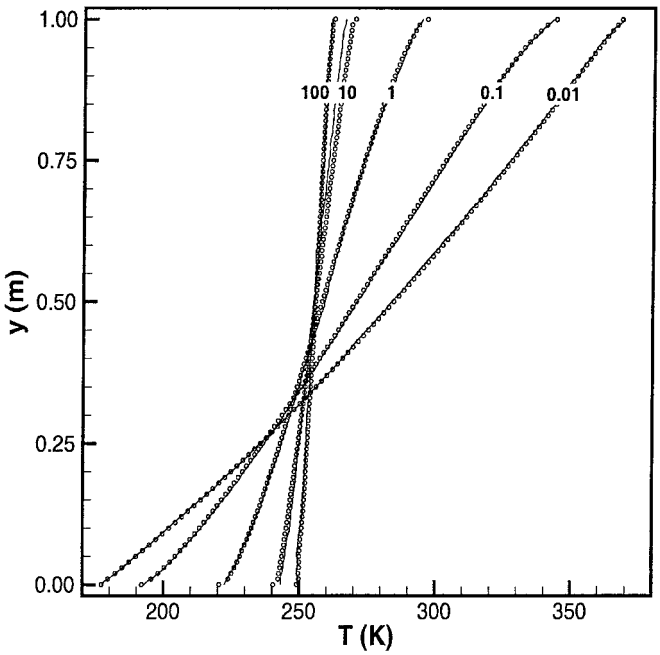

FIG. 4. The temperature profile for the thermal Couette flow at different Knudsen numbers (Kn = 0.01, 0.1, 1, 10, 100 as labeled in the plot; circle: IP, line: DSMC).

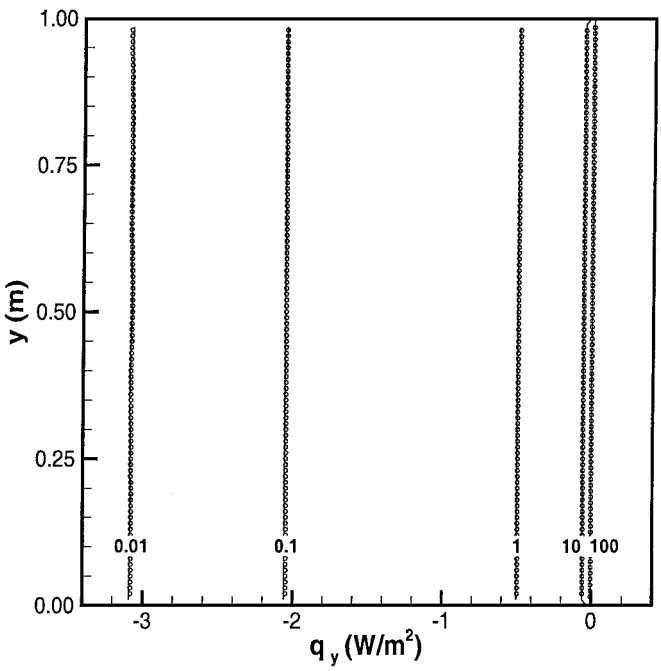

FIG. 5. The heat flux profile for the thermal Couette flow at different Knudsen numbers (Kn = 0.01, 0.1, 1, 10, 100 as labeled in the plot; circle: IP, line: DSMC).

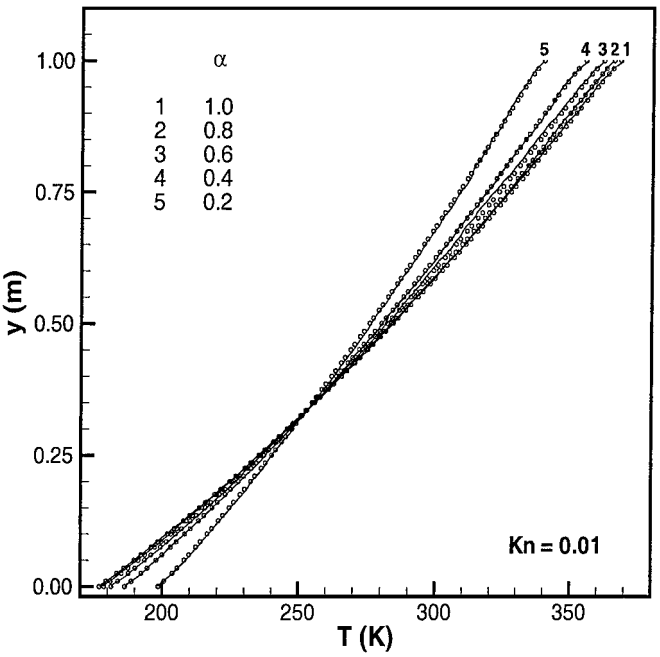

FIG. 6. The temperature profile for the thermal Couette flow under different wall conditions when Kn = 0.01 (thermal accommodation coefficient $\alpha = 1.0, 0.8, 0.6, 0.4, 0.2$ for both plates; circle: IP, line: DSMC).

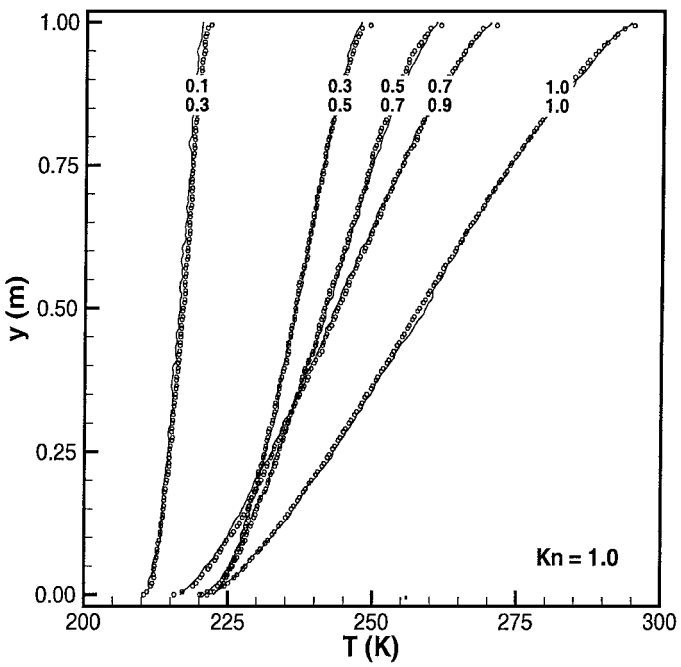

FIG. 7. The temperature profile for the thermal Couette flow under different wall conditions when Kn = 1.0 (thermal accommodation coefficient $\alpha_1 = 1.0, 0.9, 0.7, 0.5, 0.3$ for the plate at $y = 0$ m, and $\alpha_2 = 1.0, 0.7, 0.5, 0.3, 0.1$ for the plate at $y = 1$ m; circle: IP, line: DSMC).

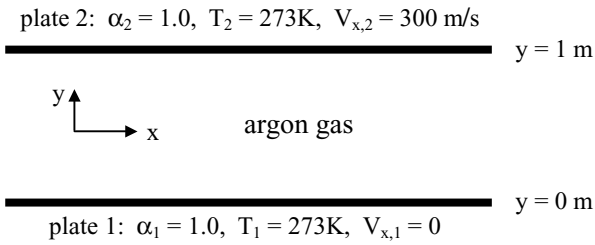

FIG. 8. Schematic diagram for the high speed Couette flow.

Because of the large velocity gradient, the dissipation causes the gas temperature to increase significantly, which requires the thermal conductivity and the dissipation to be balanced to reach a steady-state condition.

Figure 8 shows the flow between two plates with one at rest and the velocity of the other is 300 m/s. The temperature of both plates is 273 K. A similar case (Kn = 0.00925) can be found in Bird's book with detailed analysis [8]. In the current simulation, the IP method is examined for flows ranging from the near-continuum regime to the free-molecular regime. Excellent agreement between the IP results and the DSMC results is obtained for the velocity profiles as can be seen from Fig. 9. Figure 10 shows that the agreement for the temperature profile is also very good except that the DSMC results exhibit some statistical scatter. The shear stress distribution between the plates is plotted in Fig. 11. There is a small difference of 2% between the IP results and the DSMC results. As stated in Bird's book [8], the shear stress (0.00624 N/m^2) obtained from the DSMC method for the case with Kn = 0.00925 is a little lower than expected (0.00639 N/m^2). For the case with Kn = 0.01 in Fig. 10,

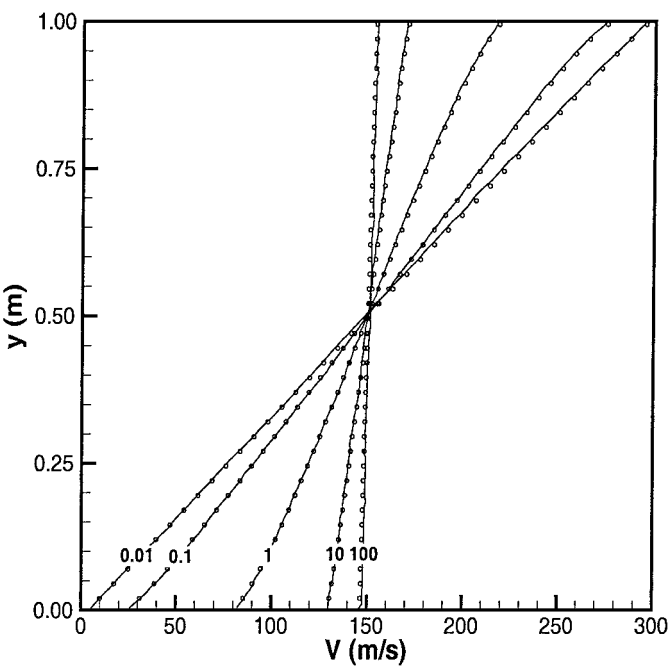

FIG. 9. Velocity profile for the Couette flow at different Knudsen numbers (Kn = 0.01, 0.1, 1, 10, 100 as labeled in the plot; circle: IP, line: DSMC).

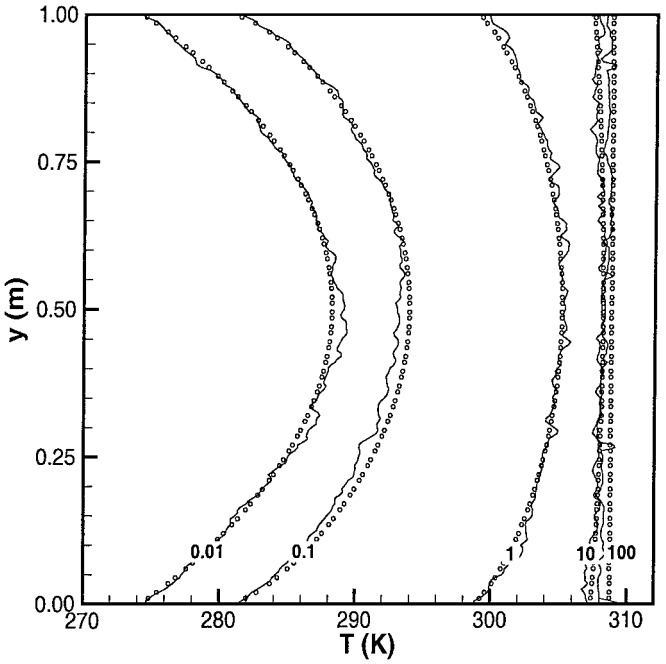

FIG. 10. The temperature profile for the Couette flow at different Knudsen numbers (Kn = 0.01, 0.1, 1, 10, 100 as labeled in the plot; circle: IP, line: DSMC).

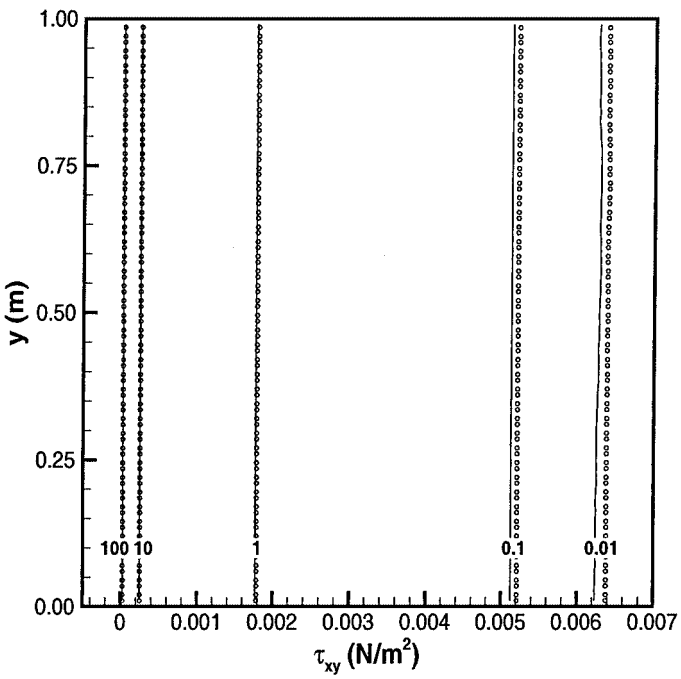

FIG. 11. The shear stress profile for the Couette flow at different Knudsen numbers (Kn = 0.01, 0.1, 1, 10, 100 as labeled in the plot; circle: IP, line: DSMC).

compared with the DSMC data (0.00626 N/m^2), the IP method predicts an average shear stress of 0.00639 N/m^2.

3.3. Rayleigh Flow

The above examples involve steady flows. The Rayleigh flow is an unsteady flow in which a plate below a gas at rest suddenly acquires a constant parallel velocity and a constant temperature. In Fig. 12, the argon gas is at rest at $t = 0$ with a temperature of 273 K. When $t > 0$, the plate obtains a constant velocity 10 m/s and a constant temperature 373 K. There is an analytical solution to the Rayleigh flow for times much less than the mean collision time τ_0 ($\tau_0 = \lambda/v_m$, where v_m is the mean molecular speed with $v_m = \sqrt{8RT/\pi}$) [7]:

$$\frac{n}{n_\infty} = \frac{1}{2}\left[\left\{1 + \operatorname{erf}\left(\frac{\beta_\infty y}{t}\right)\right\} + \left(\frac{T_\infty}{T_w}\right)^{1/2} \operatorname{erfc}\left(\frac{\beta_w y}{t}\right)\right] \tag{41}$$

$$V_x = \frac{1}{2} V_{x,w}\left(\frac{T_\infty}{T_w}\right)^{1/2} \operatorname{erfc}\left(\frac{\beta_w y}{t}\right) \Big/ \left(\frac{n}{n_\infty}\right) \tag{42}$$

$$V_y = \frac{1}{2\pi^{1/2}\beta_\infty}\left\{\exp\left(-\frac{\beta_w^2 y^2}{t^2}\right) - \exp\left(-\frac{\beta_\infty^2 y^2}{t^2}\right)\right\} \Big/ \left(\frac{n}{n_\infty}\right) \tag{43}$$

$$T = T_\infty\left[1 + \frac{1}{2}\operatorname{erfc}\left(\frac{\beta_w y}{t}\right)\left(\frac{T_\infty}{T_w}\right)^{1/2}\left(\frac{T_w}{T_\infty} - 1\right) \Big/ \left(\frac{n}{n_\infty}\right)\right] + \frac{y}{t}\frac{V_y}{3R} + \frac{V_{x,w} \cdot V_x}{3R} - \frac{1}{3R}\left(V_x^2 + V_y^2\right), \tag{44}$$

where $\beta = (2RT)^{-1/2}$, $\beta_w = (2RT_w)^{-1/2}$, erf( ), and erfc( ) are the error function and the complementary error function, respectively.

Figure 13 shows the simulated results at $t = 0.01\tau_0$ from the IP and the DSMC methods along with the analytical solution. Clearly, the DSMC results agree well with the analytic solution, while the IP results fail except for the parallel velocity distribution. This is because all particles in the IP implementation carry the same energy when they leave the plate. However, when molecules leave the plate, those molecules with larger thermal velocity carry more energy; thus the energy transferred from the plate can be carried further into the gas. Therefore, for the region far from the plate ($y > 0.3$ m), the temperature predicted by the IP method is smaller than the analytic result, while it is higher than the analytic result for the near plate region ($y < 0.3$ m). The density profile and normal velocity profile are affected by the wrong temperature profile in the IP method, while the parallel velocity profile is correct since the IP implementation only affects the energy transport.

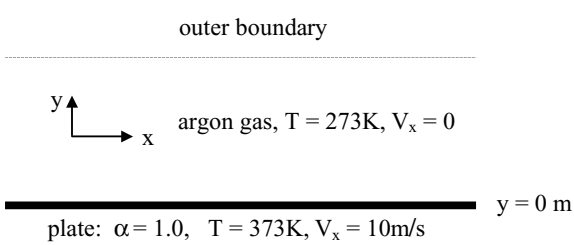

FIG. 12. Schematic diagram for the Rayleigh flow.

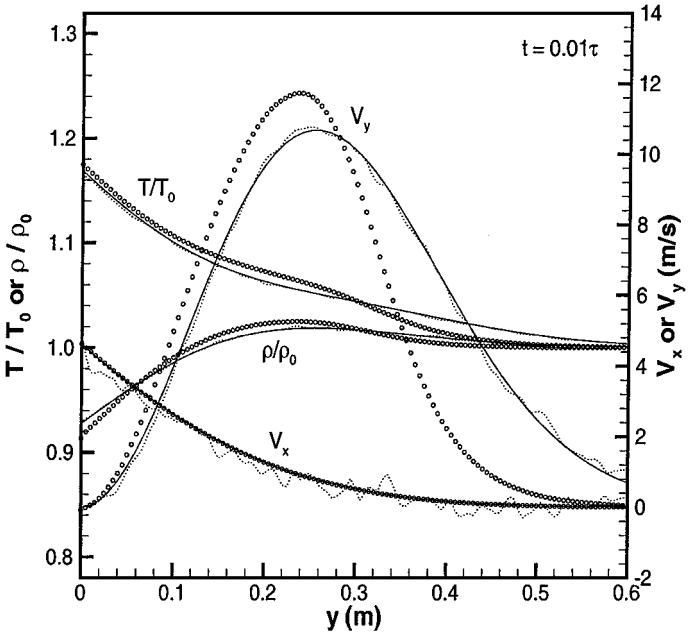

FIG. 13. Profiles for the Rayleigh flow at $t = 0.01\tau_0$ (circle: IP, dot line: DSMC, solid line: collisionless flow theory [7]).

The above situation is improved as the time increases (Figs. 14–17). When time $t = 10\tau_0$, the particles undergo 10 collisions on average. Thus the effect of random movements of the particles reflected from the plate is decreased due to collisions. Hence, the implementation of the IP method tends to be correct when there are enough collisions. Figure 17 shows that

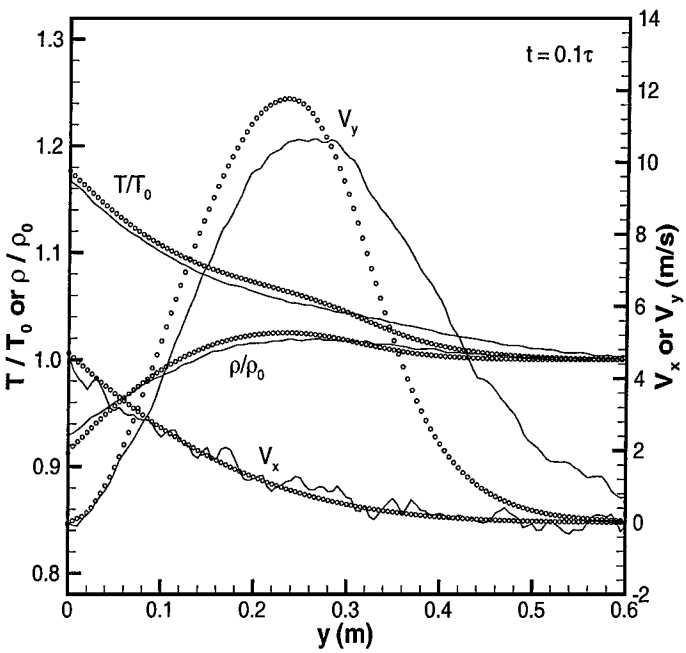

FIG. 14. Profiles for the Rayleigh flow at $t = 0.1\tau_0$ (circle: IP, line: DSMC).

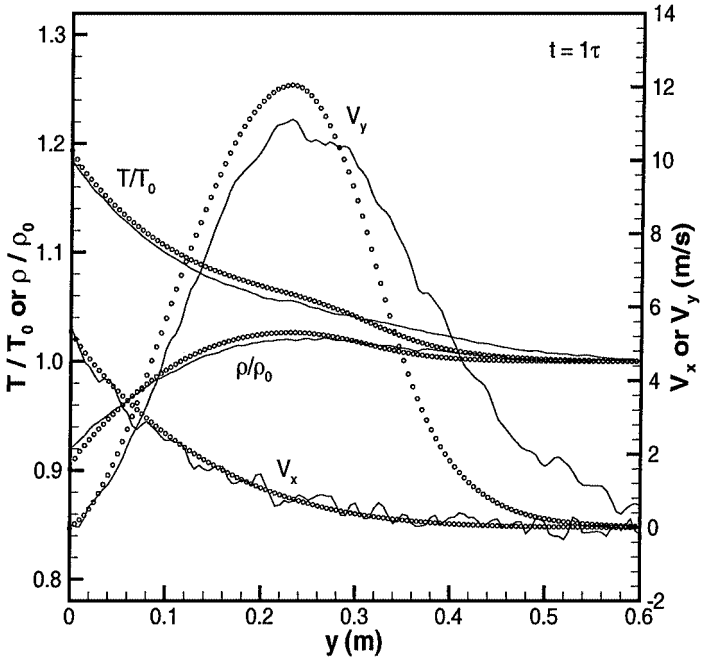

FIG. 15. Profiles for the Rayleigh flow at $t = 1\tau_0$ (circle: IP, line: DSMC).

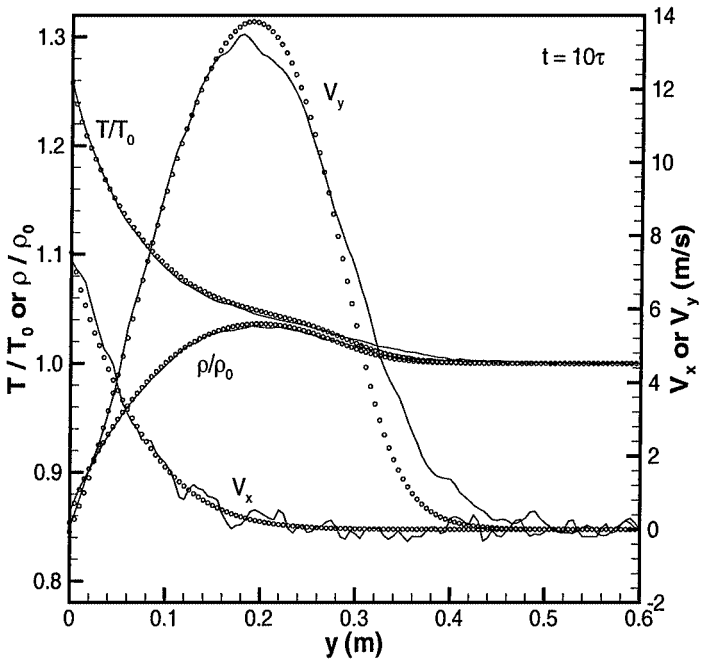

FIG. 16. Profiles for the Rayleigh flow at $t = 10\tau_0$ (circle: IP, line: DSMC).

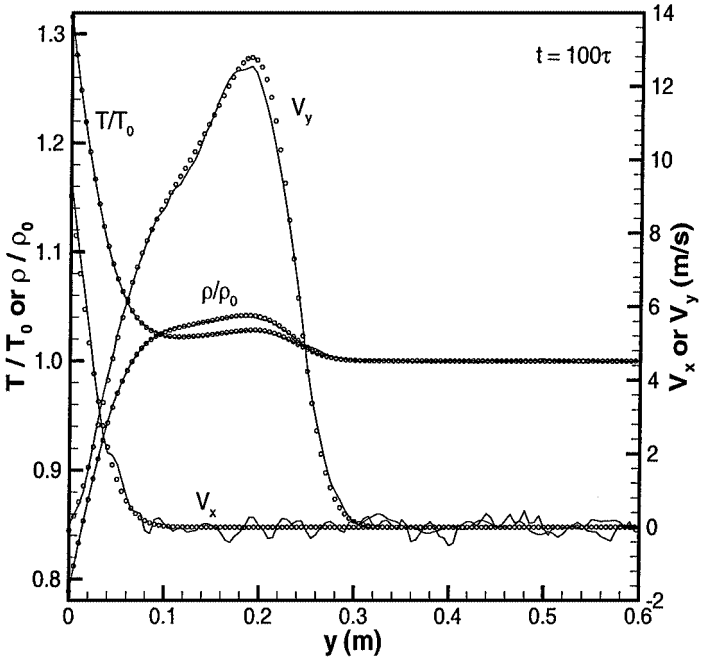

FIG. 17. Profiles for the Rayleigh flow at $t = 100\tau_0$ (circle: IP, line: DSMC).

the agreement between the IP results and the DSMC results is good when time $t = 100\tau_0$. Therefore, the additional energy transfer model works fine for this flow with small bulk velocity.

3.4. Flow over a NACA0012 Airfoil

One-dimensional flows are selected as test problems because of their well-defined properties. However, the IP method is not limited to 1D flows. In this section, an air flow around a NACA0012 airfoil with a chord length of 0.04 m is considered. The detailed flow condition is listed in Table IV, where Re_∞ and Kn_∞ are based on the chord length. Again, the selected flow velocity is not very small such that reasonable DSMC results can be obtained. Some experimental data and a Navier–Stokes solution for these conditions can be found in [18].

The computational domain is shown in Fig. 18, which uses the symmetry of the problem. The whole domain is divided into 9120 nonuniform structured cells that are clustered to the airfoil. On average, about 50 particles are located in each cell. Free stream flow conditions are applied to all the boundaries except for the symmetric line of the airfoil and the downstream boundary where a gradient boundary condition is adopted, since the computation domain is much larger than the airfoil. The time step is set to 5×10^{-8} s, which is smaller than the

TABLE IV
Free Stream Conditions for Flow over a NACA0012 Airfoil

Ma_∞	Re_∞	Kn_∞	L_{chord} (m)	ρ_∞ (kg/m^3)	U_∞ (m/s)	T_∞ (K)	T_w (K)
0.8	73	0.014	0.04	1.116×10^{-4}	257	257	290

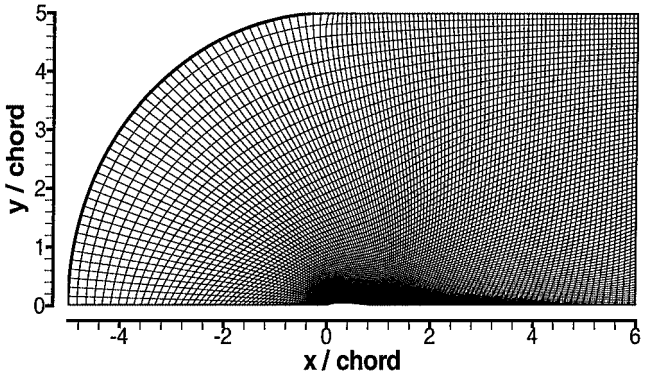

FIG. 18. Computational grids for flow over a NACA0012 airfoil.

mean collision time of particles. To reach the steady state, 30,000 iterations are executed before the flow field is sampled.

Figures 19 and 20 show the density contours nondimensionalized by the free stream density. The total sample size used in the DSMC and the IP results is about 450,000 particles per cell. However, the contours in the DSMC results are still not smooth because of the statistical scatter. The simulated density distributions exhibit the same basic features in both methods. The agreement between the density fields around the airfoil from the two methods is excellent. It is also important to examine the surface properties of the airfoil obtained from the two methods. Figure 21 shows the slip velocity distributions for both methods. Here, the slip velocity is the flow velocity of the air attached to the wall. A comparison of the pressure on the airfoil surface from the methods is shown in Fig. 22. Figure 23 shows

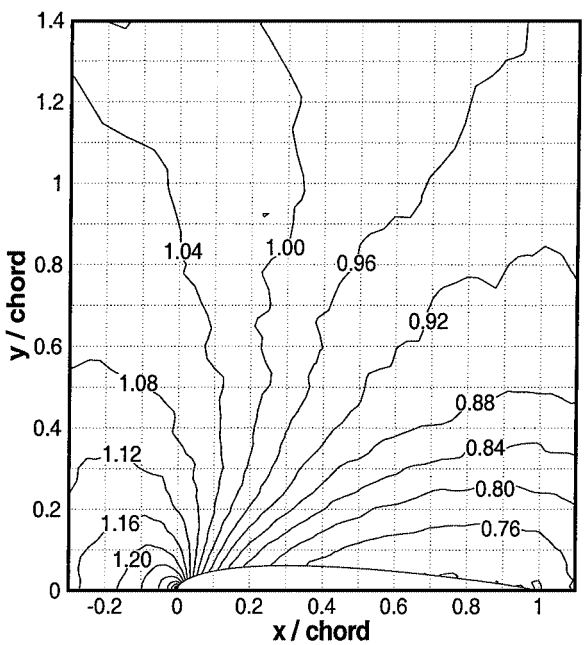

FIG. 19. Density flow field (ρ/ρ_∞) from the DSMC method for flow over a NACA0012 airfoil.

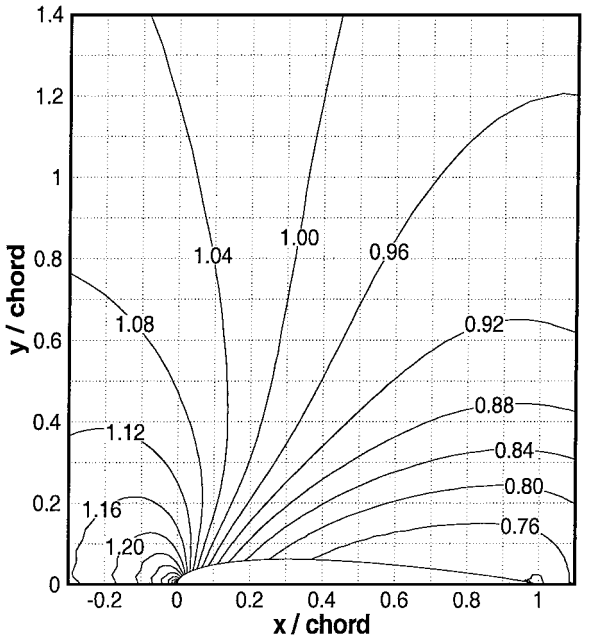

FIG. 20. Density flow field (ρ/ρ_∞) from the IP method for flow over a NACA0012 airfoil.

the shear stress distributions on the surface for the DSMC and the IP methods. Again, very good agreement is obtained between the IP and the DSMC methods throughout these plots. It would be very interesting to compare the temperature profiles from both methods to check the validity of the additional energy transfer model for this flow with large bulk velocity.

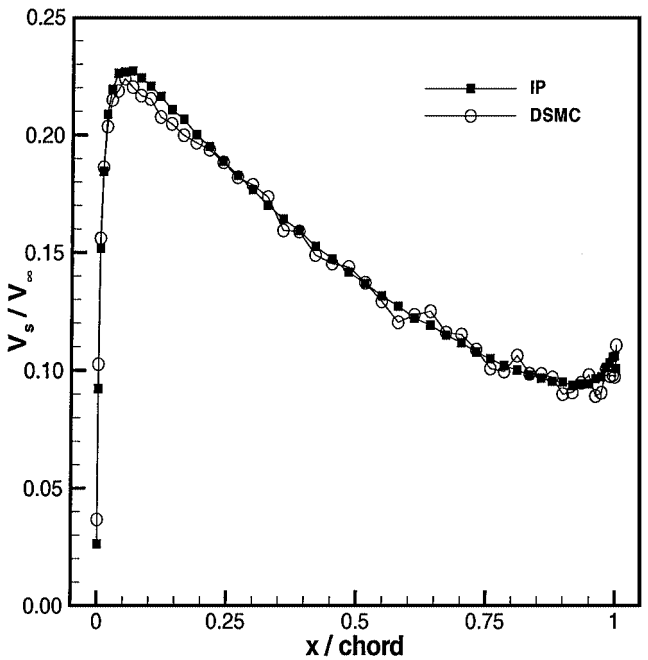

FIG. 21. Comparison of the slip velocity distributions for flow over a NACA0012 airfoil.

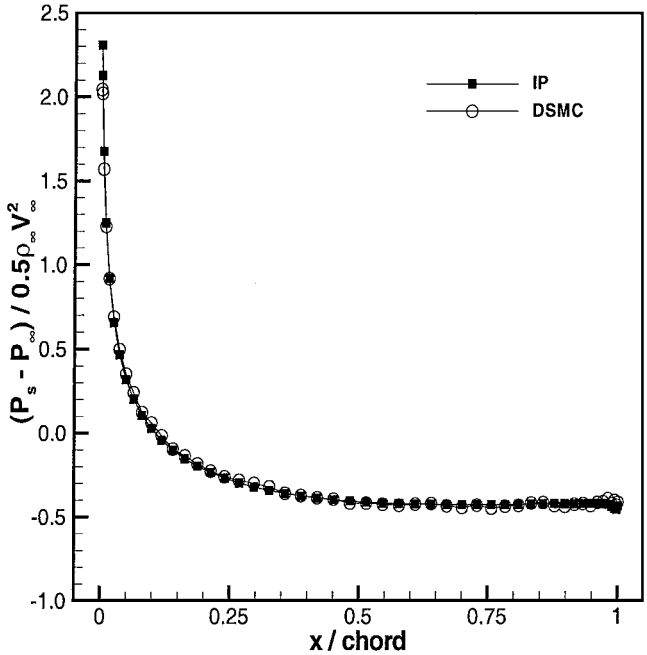

FIG. 22. Comparison of the surface pressure distributions for flow over a NACA0012 airfoil.

However, a huge sampling size is needed to obtain a smooth temperature profile for the DSMC method. Although a comparison of the temperature is impossible for this problem, the good agreement of other properties between the IP and the DSMC methods shows that the additional energy transfer model can be accepted for flows with large bulk velocity.

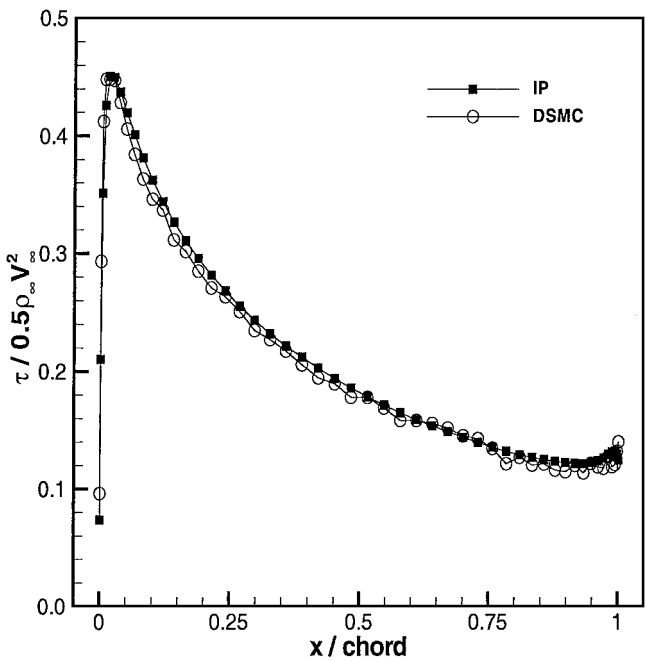

FIG. 23. Comparison of the shear stress distributions on the surface for flow over a NACA0012 airfoil.

IV. CONCLUSIONS

In this paper, the information preservation method was developed and tested for several rarefied gas flows. The IP method was established by an assumption that the macroscopic information of the flow field can be preserved by the DSMC particles. The development of the macroscopic information was obtained through a collision and movement step and a modification step. Also an approximate physical model (additional energy transfer model) and a phenomenological model (collision model) were proposed to describe the momentum and energy transfers for the IP method.

The IP method was proposed to solve kinetic problems. However, the foundation of the IP method has not been mathematically proved. The correctness of the method was tested by several rarefied gas flows. Four simulation examples showed the validity of the IP method. The IP method predicted very good results for the thermal Couette flows and the high speed Couette flows ranging from the near-continuum regime to the free-molecular regime. The example of a transonic flow over a NACA0012 airfoil also showed that the IP method performed well for general 2D steady flows. The Rayleigh flows, however, showed the proposed IP implementation was good for unsteady flows only when each particle underwent enough collisions, which means the IP method was also good for low frequency unsteady flows. Hence, it is concluded that the IP method can be applied to general 2D steady and low frequency unsteady flows.

ACKNOWLEDGMENT

The authors appreciate the support from the Air Force Office of Scientific Research through MURI Grant F49620-98-1-0433.

REFERENCES

1. C. M. Ho and Y. C. Tai, Micro-electro-mechanical-systems (MEMS) and fluid flows, *Annu. Rev. Fluid Mech.* **30**, 579 (1998).
2. M. Gad-el-Hak, The fluid mechanics of microdevices—The Freeman scholar lecture, *J. Fluids Eng.* **121**, 5 (1999).
3. E. Arkilic, M. A. Schmidt, and K. S. Breuer, Gaseous slip flow in long microchannels, *J. Micro Electro Mech. Systems* **6**, 167 (1997).
4. S. Fukui and R. Kaneko, Analysis of ultra thin gas film lubrication based on linearized Boltzmann equation: First report—Derivation of a generalized lubrication equation including thermal creep flow, *J. Tribol.* **110**, 253 (1988).
5. A. Beskok and G. E. Karniadakis, A model for flows in channels, pipes and ducts at micro and nano scale, *Microscale Thermophys. Eng.* **3**, 43 (1999).
6. R. L. Bayt and K. S. Breuer, Viscous effects in supersonic MEMS-fabricated micronozzles, in *Proceedings of the 1998 ASME International Mechanical Engineering Congress and Exposition, Anaheim, CA*, 1998.
7. G. A. Bird, *Molecular Gas Dynamics* (Clarendon, Oxford, 1976).
8. G. A. Bird, *Molecular Gas Dynamics and the Direct Simulation of Gas Flows* (Clarendon, Oxford, 1994).
9. E. P. Muntz, Rarefied gas dynamics, *Annu. Rev. Fluid Mech.* **21**, 387 (1989).
10. G. A. Bird, Recent advances and current challenges for DSMC, *Comput. Math. Appl.* **35**(1), 1 (1998).
11. E. S. Oran, C. K. Oh, and B. Z. Cybyk, Direct simulation Monte Carlo: Recent advances and applications, *Annu. Rev. Fluid Mech.* **30**, 403 (1998).

12. J. Fan and C. Shen, Statistical simulation of low-speed unidirectional flows in transition regime, in *Rarefied Gas Dynamics*, edited by R. Brun *et al.* (Cepadus-Editions, Toulouse, 1999), Vol. 2, p. 245.
13. J. Fan and C. Shen, Statistical simulation of low-speed rarefied gas flows, *J. Comput. Phys.* **167**, 393 (2001).
14. L. S. Pan, G. R. Liu, B. C. Khoo, and B. Song, Modified direct simulation Monte Carlo method for low-speed microflows, *J. Micromech. Microeng.* **10**(1), 21 (2000).
15. L. S. Pan, T. Y. Ng, D. Xu, and K. Y. Lam, Molecular block model direct simulation Monte Carlo method for low velocity microgas flows, *J. Micromech. Microeng.* **11**, 181 (2001).
16. C. Cai, I. D. Boyd, J. Fan, and G. V. Candler, Direct simulation methods for low-speed microchannel flows, *J. Thermophys. Heat Transfer* **14**(3), 368 (2000).
17. I. D. Boyd and Q. Sun, Particle simulation of micro-scale gas flows, AIAA-01-0876 (Reno, 2001).
18. J. Fan, I. D. Boyd, C. P. Cai, K. Hennighausen, and G. V. Candler, Computation of rarefied flows around a NACA 0012 airfoil, *AIAA J.* **39**(4), 618 (2001).
19. S. Dietrich and I. D. Boyd, Scalar and parallel optimized implementation of the direct simulation Monte Carlo method, *J. Comput. Phys.* **126**, 328 (1996).
20. C. Shen, J. Z. Jiang, and J. Fan, Information preservation method for the case of temperature variation, in *Rarefied Gas Dynamics*, edited by T. J. Bartel and M. A. Gallis (American Institute of Physics, Melville, 2001), p. 185.
21. Q. Sun, I. D. Boyd, and J. Fan, Development of an information preservation method for subsonic, micro-scale gas flows, in *Rarefied Gas Dynamics*, edited by T. J. Bartel and M. A. Gallis (American Institute of Physics, Melville, 2001), p. 547.
22. S. Chapman and T. G. Cowling, *The Mathematical Theory of Non-Uniform Gases*, 3rd ed. (Cambridge Univ. Press, Cambridge, UK, 1970).
23. T. I. Gombosi, *Gaskinetic Theory* (Cambridge Univ. Press, Cambridge, UK, 1994).